

Article

Sand Net Device to Control the Meanders of a Coastal River: The Case of the Authie Estuary (France)

Anh T. K. Do ^{1,2,*}, Nicolas Huybrechts ¹  and Philippe Sergent ¹

¹ Cerema, HA Research Team, 134 rue de Beauvais, 60200 Compiègne, France; nicolas.huybrechts@cerema.fr (N.H.); Philippe.Sergent@cerema.fr (P.S.)

² Faculty of Water Resources Engineering, The University of Da Nang (UD)—University of Science and Technology, 54 Nguyen Luong Bang Str, Danang 50000, Vietnam

* Correspondence: dtkanh@dut.udn.vn or thi-kim-anh.do@cerema.fr

Abstract: The Authie estuary is characterized by an important southern sand spit and a northern shoreline subject to strong erosion due to the meandering of the coastal river. In order to reduce this erosion, a new soft coastal defence, namely the sand net device (SND), has been implemented inside the Authie estuary. It consists of several nets assembled in an inverted V creating a porous structure and thus trapping sand as shoreline protection. However up to now, little proof has been provided on the explicit influence of this SND on the hydrodynamic pattern and associated morphodynamics. In this paper, field surveys of morphological developments combined with numerical modelling (Telemac-2D/3D) analyze the influence of the SND into flow pattern and morphodynamics. In situ monitoring clearly points out sedimentation around the SND and a deepening of the main channel. Modelling results show that, without SND, erosion is observed around its location. With a SND implemented, the velocity has been reduced and created a deviation in its direction by a circulation around the SND location. The impact area of the structure is around 500 m in both directions, upstream and downstream part.

Keywords: sand net device; Authie estuary; meandering river; erosion; sedimentation



Citation: Do, A.T.K.; Huybrechts, N.; Sergent, P. Sand Net Device to Control the Meanders of a Coastal River: The Case of the Authie Estuary (France). *J. Mar. Sci. Eng.* **2021**, *9*, 1325. <https://doi.org/10.3390/jmse9121325>

Academic Editors: Marissa Yates, Jennifer Brown and Pushpa Dissanayake

Received: 16 June 2021

Accepted: 19 July 2021

Published: 23 November 2021

Publisher's Note: MDPI stays neutral with regard to jurisdictional claims in published maps and institutional affiliations.



Copyright: © 2021 by the authors. Licensee MDPI, Basel, Switzerland. This article is an open access article distributed under the terms and conditions of the Creative Commons Attribution (CC BY) license (<https://creativecommons.org/licenses/by/4.0/>).

1. Introduction

Estuary mouths generally feature complex interactions between waves, tides, wave-induced currents that vary with tidal range and fluvial discharge. These systems disrupt the longshore drift and sediment supply [1]. Along sandy coasts, estuary mouths are often characterized by sand accumulation in the form of sand bars or of a sand spit that develops across the estuary [2,3]. The continuing development of a spit across the estuary mouth, usually in the direction of the prevailing littoral drift, frequently results in the erosion of the downdrift estuary shore due to the migration of the main estuary channel [4]. In addition to the effects of natural forcing factors, sediment accumulation and/or shore erosion at an estuary mouth can be increased or be conversely reduced due to human actions that modify estuarine hydrodynamics and sediment dynamics (man-induced changes in river discharge, land reclamation, river bank stabilization, coastal defense structures) [5].

One typical example of interaction between coastal sand spit and neighbouring river is the shallow Authie estuary located in the English Channel (Figure 1a). The Authie mouth consists of an important south sand spit prograded seawards and northward and a north bank subject to strong erosion, and a large zone of saltmarshes in the middle part of the estuary. This estuarine mouth is largely blocked by the prominent sand spit and intertidal/subtidal platform, and this has forced the main channel to migrate along the northern shore and adjacent shoreline [4].

The last severe dune erosions of Authie estuary occurred in 2011 and 2018. The meander has approached the northern shore and eroded the dunes under the combined action of currents and waves [6]. In order to prevent such events, a new soft coastal defence system

has been implemented to reduce erosion inside the Authie estuary. It consists of a porous groyne which aims to trap sediment inside net layers and to thus create a sandy deposit as shoreline protection. Up to now, the efficiency of this sand net device (SND) has not been documented. The objective of this contribution is thus to analyze the influence of this SND on the flow pattern and morphodynamic of the estuary. The characteristics of the studied configuration and the implemented SND are first presented. The SND influence is studied with field surveys combined with numerical modelling. Field survey allows to quantify the bed evolution around the implemented device. A 3D numerical flume experiment is developed to characterize the drag coefficient induced by the SND. Finally, a 2D large scale model of the estuary serves to analyse the morphodynamic evolution and the impact on flow circulation with or without the SND in order to highlight its effects.

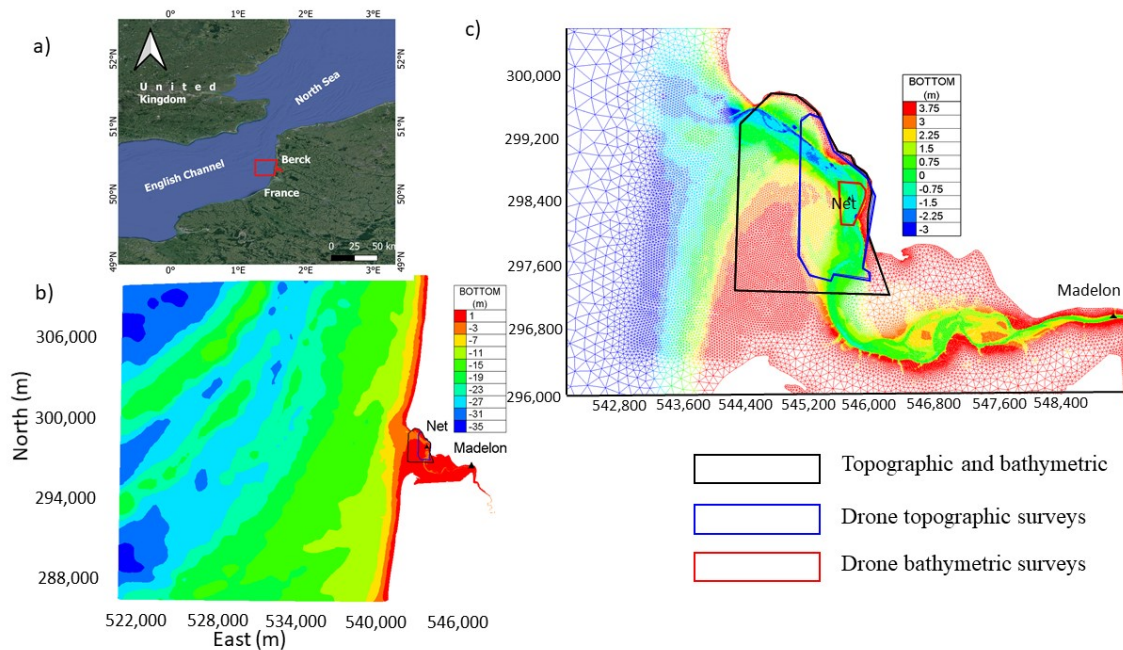


Figure 1. Location of Authie estuary and survey stations (a); model domain in numerical model (b); and areas of topographic and bathymetric surveys (c).

2. Authie Estuary

The Authie Estuary, located in the eastern English Channel near the town of Berck-sur-Mer (Figure 1a), is a small macrotidal estuary exhibiting a relatively large intertidal zone. The total length of the main river is 98 km and the river drains a low-gradient Mesozoic limestone plateau catchment of approximately 985 km² that supplies very limited sediment to the coastal zone due to the nature of the bedrock geology [4,7]. The river discharge is quite low and ranging from 4 m³/s in summer to 13 m³/s in spring with an average of 10 m³/s [7]. The estuary mouth is affected by large tidal range within 8.5 m and 4.9 m for spring and neap tides, respectively. This large tidal amplitude is responsible for strong tidal currents up to 1 m/s at the mouth during spring tides and even up to 1.5 m/s seaward of the estuary mouth and in the adjacent coastal zone [8,9]. The tidal ranges decrease to 4 m and 1.8 m, respectively, 7 km inland (at La Madelon harbour). The coastal/nearshore zone is characterized by a shore-parallel circulation dominated by northward-directed flood currents [10].

The Authie estuary has endured infilling of sand from the English Channel [7,8,11] and describes a typical geomorphological structure. The coast to the south has both prograded seawards and northwards over time (6.1 m/yr between 2005–2012; ref. [4,7]) and the northward progradation has been accompanied by the development of a very extensive intertidal and subtidal platform and spit. The progressive extension of this

major accumulation protects the inner estuary from wave action and it thus favors the development of mudflats and saltmarshes [12]. The estuary mouth is largely blocked by the prominent sand spit and intertidal/subtidal platform, and this has forced the main channel of the Authie to flow along the northern shore of the estuary mouth and adjacent shoreline [4]. The dune erosion at the northern shoreline (Figure 2a) is induced by river meandering [6]. Large portions of the inner estuary have been polderized during the last centuries, which resulted in increased sedimentation and seaward saltmarsh progression [7,8].

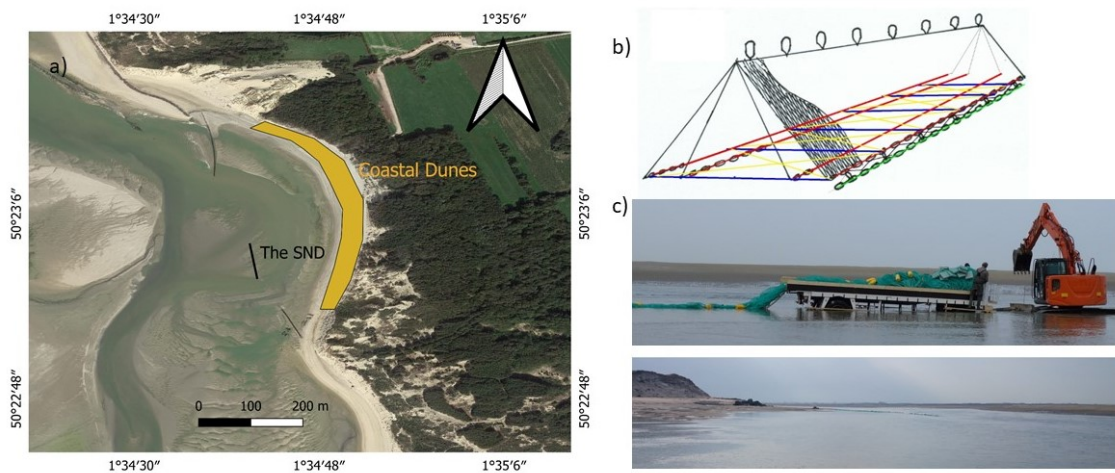


Figure 2. Location of the SND (a); schematic of the device: layers of nets assembled in inverted V, buoy to raise the device with the tide (b); and the SND in reality (c).

3. Materials and Methods

3.1. Large Scale Demonstrator of Sand Net Device (SND)

The implemented hydraulic structure (Figure 2a) is a soft engineering solution developed by the company S-Able by Michon [13], which applied for the patent. It consists of several nets assembled looking as a pyramid or a tepee to create a porous structure and associated turbulent dissipation (Figure 2b). The feet of the nets are maintained by chains and anchors, whereas the deployment of the net head on rising and falling tide is completed by floating buoys (Figure 2c). As discussed by Sergent et al. [6] the device may be considered as a porous groyne with two effects: shielding and sediment trapping. Between the shoreline and the sand spit, the river is usually meandering between two branches: one main channel near the sand spit and a secondary channel near the shoreline. The river returned to the secondary branches in 2011 and 2018. The principle is thus to install the SND at the entrance of the secondary branch of the river. The reduction of the flow velocity around the nets allows sediment trapping. The sediment deposit and the additional energy losses induced in the secondary branch will favour the flow inside the main branch where we want to maintain the coastal river. The sediment accumulation thus forms a protection to reduce the erosion pattern. Such a first device was installed in 2014 and raised in 2017 [6] but with limited morphodynamic monitoring. In 2019, a new SND was installed and a more complete field monitoring has been achieved. The length of the installation is 108 m and its width 1.5 m. The installation of the sand nets inside the secondary branch was performed on 27 March in 2019. In the part near the shoreline, the nets rely on the sandbank and they are progressively introduced inside the channel using a truck having at the end of the installation wheels almost completely in the water (about 0.5–1 m in depth, Figure 2c). When the water depth is sufficiently high so that the buoys are able to raise the nets completely, the SND height reaches up to 1.1 m.

3.2. In Situ Surveys

The field monitoring consists of different types of topographic and bathymetric surveys (Table 1). The topographic monitoring is performed by drones and covers the area defined by the blue line in Figure 1c.

Table 1. The different topographic and bathymetric data.

| Data | Date of Surveys | Area | Data in the Channel of River |
|-----------------------------------|------------------|-------------------------|------------------------------|
| Topography and bathymetry | 15 February 2019 | Black line | Yes |
| Topography | 20 March 2019 | Blue line | No |
| Bathymetry | 18 April 2019 | Red line | Yes |
| Topography and bathymetry (Lidar) | 30 April 2019 | Whole bay and shoreline | No |
| Topography | 4 July 2019 | Blue line | No |
| Bathymetry | 4 July 2019 | Red line | Yes |
| Topography | 2 September 2019 | Blue line | No |

The drone monitoring provides Digital Elevation Models (DEMs) in the right bank of Authie from the river to beyond the summit of the dune and in the left bank of Authie from the river until the end of the defined area. A first survey was carried out before the installation of the SND: 20 March 2019. Other drone surveys have occurred on 4 July 2019 and 2 September 2019.

The DEMs are constructed from drone flight involving the measurement of grounding points for the georeferencing of topographic measurements. The main channel of the Authie estuary, located in the middle, is permanently immersed (i.e., at low tide) and it is not covered. The expected accuracy of the DEMs is 5–10 centimetres (horizontal or vertical) outside the vegetated area and up to 25 cm (horizontally) on the left bank of the Authie.

As the drone sensor is blind below the water surface, the topography is completed by observations of bathymetry around the riverbed. Two surveys have been conducted in February and October 2019 (black line in Figure 1c) whereas more local surveys around the nets have been conducted in April and July 2019 (red line in Figure 1c). The different bathymetry surveys have been conducted with a single beam sounder mounted on a vessel. In addition, an airborne Lidar survey has been conducted by local authorities in April 2019. The Lidar survey covers the whole bay of Authie and the shoreline from Bay of Somme to bay of Canche. Bed elevation in both intertidal and subtidal areas are measured by the airborne sensor.

Besides, tide and velocity measurements were conducted in 2017 and 2019. The most complete data was collected in 2017 with both velocity and water level whereas only water levels were measured in 2019. Water levels are measured at two locations within Authie estuary (Net and Madelon see Figure 1c) and velocity data are available near the location of the SND.

3.3. Numerical Experiments

Two different models are set up using the open source TELEMAC-MASCARET modelling system (hereafter the TMS, version V8P1). The TMS has been widely used to simulate the hydrodynamic flow and associated sediment transport dynamic in fluvial zones [14,15] or coastal areas [16–18]. Trials have been performed inside an experimental flume (Ifremer at Boulogne sur Mer) of 4 m wide. The water depth has been remained constant at 2 m and the upstream flow velocity has been imposed from 0.6 to 1 m/s. The drag coefficient has been estimated from a force measurement on the device. However, to estimate how the drag coefficient of the SND evolves with the tidal range, numerical experiments are conducted. The studied SND in both experimental and numerical flume is similar as the one deployed in situ: 1.5 m in baseline length and 1.1 m in height.

The dimension of the numerical domain is 200 m in length, 4 m in width. The numerical model is based on Telemac 3D which solves the Navier-Stokes equations. Concerning the turbulence model, the k- ϵ model is selected. The distance between the nodes is about

0.1 m in the horizontal planes and with 18 sigma planes uniformly distributed for the vertical resolution. The same number of planes is used for all the simulations. On similar configurations, Tassi et al. [19] points out that the mesh convergence is reached for 18 planes. A simulation has been performed with 24 planes and the differences in the variables (depth and velocity) are lower than 1%.

The time step is 0.05 s and the duration of each simulation is 30 min to reach a steady flow. In the numerical model, the SND is considered as a bottom step without permeability. It serves to provide a first simple estimation of the energy losses induced by the sand net device. In reality, it could correspond to a device full of sandy deposit. As boundary condition, the velocity is imposed upstream whereas the water depth is imposed downstream. The velocity is kept constant to 0.8 m/s whereas six different values of the water depth ranging between 0.9 and 6 m are imposed in order to analyze how the drag coefficient evolves with the tidal level. The drag coefficient is estimated as

$$C_d = \frac{p_{t1} - p_{t2}}{0.5\rho U_1^2} \quad (1)$$

where p_{t1} , p_{t2} are the total pressure upstream and downstream the SND; C_d is the drag coefficient; ρ is water density and U_1 is the velocity upstream.

3.4. Large-Scale Numerical Model

The hydrodynamic model (TELEMAC-2D) is based on the depth-averaged shallow water equations for momentum and continuity [20]. The unstructured model mesh, created using Bluekenue grid generation software has variable resolution, being relatively fine (8–10 m) around the SND and coarser (200–250 m) at offshore parts. The horizontal grid contains 80.305 nodes and 158.189 triangular elements.

The computational domain of the model has been developed to represent the Authie estuary which includes the open sea (23 km in wide and 24 km in length), the estuary and a part of the upstream river (Figure 1b). The model has been forced here with tidal elevations and tidal velocities at the offshore boundaries and a constant river flow rate of 10 m³/s at the inland river boundary.

At the maritime boundary, astronomical tide elevation and tidal currents are reconstructed using the European Shelf atlases (TXPO, ref. [21]) as a superposition of harmonic waves [22] for each of the nodes of the offshore boundary (Equation (2)).

$$H_{tide} = H_0 + \sum_n H_n f_n \cos(\sigma_n t - g_n + V_n - u_n) \quad (2)$$

where H_{tide} is the tidal height; H_0 is the mean height of the water level; n is the harmonics number; H_n is the mean amplitude of the n -wave; f_n is the nodal correction for the amplitude; σ_n is the frequency; t is the time; g_n is the phase lag of the equilibrium tide; V_n is the astronomic argument; and u_n is the nodal correction for the phase lag. Similar relationships are used for the velocity.

The bathymetry interpolated on the mesh comes from different sources: offshore from the SHOM (Service Hydrographique Marine), Lidar data collected in April 2019 nearshore and inside the bay. More detailed bathymetric data inside the estuary area and the net area is used (survey of February 2019). During the simulations, a time step of 5 s is used for all the simulations. An initial spin-up simulation of 30 days is achieved to initialize the hydrodynamic variables.

The sediment transport module (GAIA), Audouin et al. [23] is internally coupled with the hydrodynamics (TELEMAC-2D). The bed friction is predicted using the bed roughness prediction by van Rijn. [24]. The Soulsby-van Rijn transport formula [25] is used here to estimate the total transport rate (bed load + suspended load) without considering bed slope correction and morphological factor. The total bed roughness can be decomposed into a

grain roughness k'_s , a small-scale ripple roughness k_r , a mega-ripple component k_{mr} , and a dune roughness k_d .

$$k_s = k'_s + \sqrt{k_r^2 + k_{mr}^2 + k_d^2} \tag{3}$$

Both small scale ripples and grain roughness have an influence on the sediment transport laws, while the mega-ripples and dune roughness only contribute to the hydrodynamic model (total friction, ref. [26,27]). In the bed roughness feed-back method, the total bed roughness calculated by GAIA is sent to Telemac-2D.

Influence of waves and wind are not reckoned in this study. The SND is installed behind the sand spit and it is thus protected from the waves except during stormy events. Here, it is proposed to focus on a short-term period (1 month). For such a short-term period, the tide and the flowrate can be considered as the main forcing.

First, the hydrodynamic simulation is carried out considering a fixed bed to assess its accuracy. As proposed by Huybrechts et al. [16,17], no calibration is performed since the friction coefficients are provided by the van Rijn formula. Then, the hydrodynamic model is coupled with sediment transport and morphological evolution. The results of the fixed bed simulation are used as initial conditions for the coupled simulation. The coupled simulation (Telemac 2D and Gaia) are conducted with and without the SND. The simulation times of all sediment transport is 45 days (3 neap-spring cycles) starting from 15 February 2019 as the initial bathymetry before net implementation.

The presence of structure is often treated by an additional drag force for instance for tidal turbines [28,29] or even for bridge piers [20]. Similarly it is proposed to reckon the energy losses induced by the SND by a drag force inside the model.

The position of the SND inside the mesh has been defined as a soft line meaning that nodes are placed along a defined line during the building of the mesh. The drag force is applied on these nodes using a polygon. In this way, the representation of the SND is less sensitive to the mesh resolution.

The drag force is applied as a source term added to momentum equation taking into account the orientation of the SND. The drag force equation is adjusted from Joly et al. [28]. The two components along x and y direction of drag force are indicated below.

$$F_{D,x} = -\frac{1}{2}H_{net}C_D U | U | \cos(\theta) \tag{4}$$

$$F_{D,y} = \frac{1}{2}H_{net}C_D V | U | \sin(\theta) \tag{5}$$

where C_D is a drag coefficient that can be extracted from the numerical flume experiment, θ is the orientation of the central axis of the SND, in this case $\theta = -30^\circ$ (0 is north oriented), H_{net} is the height of the net (1.1 m) and U and V are the velocity (east and north component).

The drag coefficient is assumed to be independent of the flow orientation. The flow orientation only has an influence on the final force. For a South-North oriented SND, the $F_{D,y}$ is null and the $F_{D,x}$ will be maximum for a flow-oriented East-West. More flume or numerical experiments would be necessary to build a more complete relationship of the drag coefficient (depth ratio, flow angle, ...).

4. Results and Discussion

This section first presents the results and discussions of observed morphodynamics around the SND. Second, the results of estimation of the drag coefficient by 3D numerical experiments are presented and discussed. Third, the validated results of 2D large-scale models are presented. Finally, Sections 4 and 5 are used to present and discuss about the influence of the SND on residual currents and morphodynamics based on the large-scale model. These provide valuable insight into the influence of the SND on the flow pattern and morphodynamic of the Authie estuary.

4.1. In Situ Observed Morphodynamic around the SND

Measured topographic evolutions are illustrated in (Figure 3). The location of the SND is represented by a black line. A few days before the installation of the SND (Figure 3a, 20 March), width of the river is 70 m. The sand spit is moving from west to east and it is pushing the river to the shoreline. The configuration 3 months after the installation is represented in (Figure 3b). It appears that the river width has become narrow in the vicinity of the device (width = 25 m). The sand spit on the west has also been reduced. Around the net, sedimentation has effectively occurred. Between 3 and 6 months, a more stable configuration around the net is observed. The channel seems stabilized and maintained away from the shoreline.

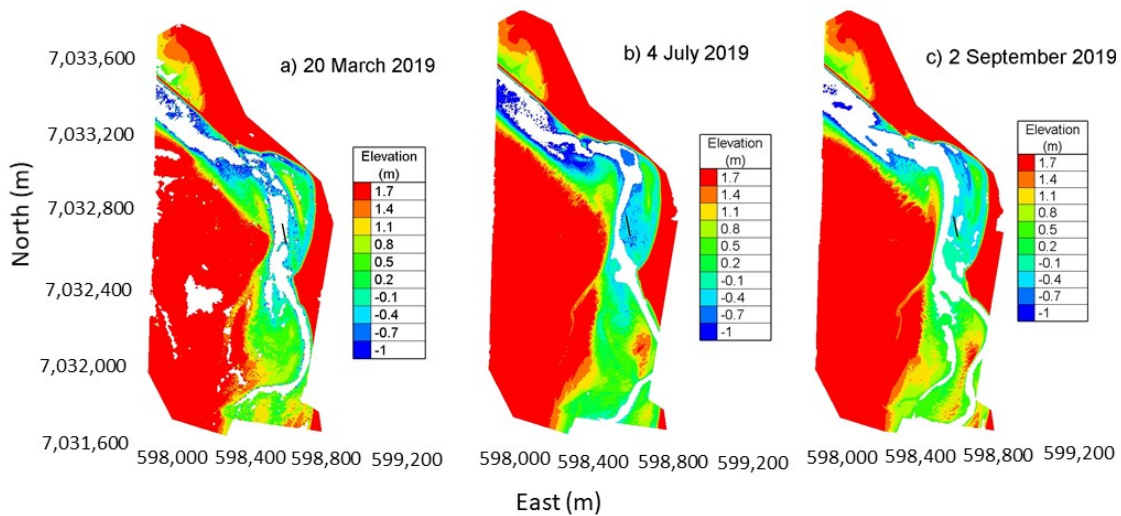


Figure 3. Topographic surveys by drone: (a) at 20 March 2019; (b) at 4 July 2019 and (c) at 2 September 2019. SND was installed 27 March 2019 indicating by the black line.

The erosion-sedimentation pattern inside the channel around SND is analyzed based on local bathymetry surveys (Figure 4). Figure 4a depicts the temporal change in the erosion/sedimentation pattern in the channel between February 2019 to October 2019 whereas Figure 4b,c display bed elevation at two cross sections, T1 downstream the nets and T2 at net location. Positive values of Dz indicates sedimentation whereas negative values indicate erosion.

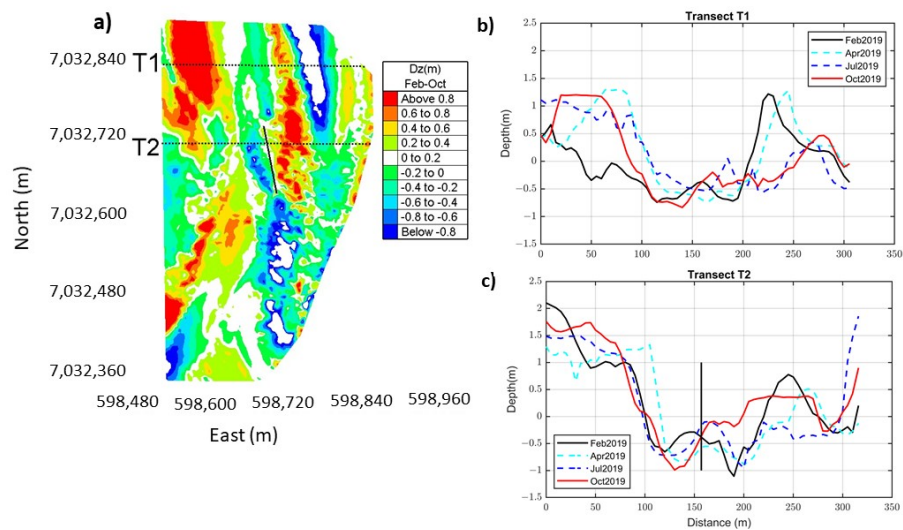


Figure 4. (a) Bed level changes during period February 2019 and October 2019; (b) Cross transect T1 and (c) Cross transect T2 at the SND. The back lines depict the location of the SND.

In Figure 4a, an important sedimentation is noticed on the east side of the SND whereas erosion has occurred at the west provides more details about the bed evolution. For T1 and T2, a growth of the sand spit is first observed between February to April. Erosion has occurred on both sides of the net during this period. In fact, this period corresponds to a mixed configuration: 1.5 months of natural evolution before the sand net installation and one month with the SND. Between April and July, sedimentation has occurred around the SND and a deepening of the channel has occurred between the net and the sand spit (Figure 4b). Between July and September, similar patterns are observed: erosion of the riverbed on the west, sedimentation on the eastern side of the SND. Figure 5 points out that these morphological changes are associated with a shift of the main channel orientation. The yellow line in Figure 5 indicates the thalweg line of -0.8 m of the main channel. In February (Figure 5a), two deep channels are observed with their junction near the net. In October (Figure 5b), only the channel at the west remains and the river is blocked between the sand spit and the sandy deposits generated around the SND.

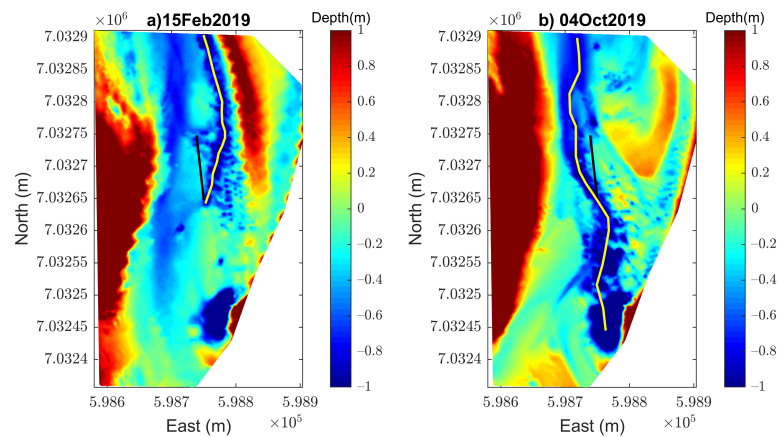


Figure 5. Detail bathymetry around the SND at: (a) 15 February 2019; (b) 4 October 2019. The yellow lines depict as the thalweg line of -0.8 m of the main channel. The back lines depict the location of the SND.

4.2. Estimation of the Drag Coefficient Induced by the SND Using the 3D Numerical Experiments

The flow pattern predicted by the 3D numerical experiments is illustrated for the 2 m depth configuration (Figure 6) for both components: along channel (X component) and vertical component (W component). Due to the step effect, the presence of the device induces a reduction of the flow section and an increase of the flow velocity. For the configuration of 2 m in water depth, the flow velocity increases from 0.8 to 2 m/s. A drop in the free surface elevation is also noticed across the SND (Figure 6). Just behind the step, a low velocity zone is present which is favorable to sedimentation. The drag coefficient estimated from the experimental flume is 3 for the 2 m depth configuration whereas it reaches 3.6 in our numerical experiment. The measured velocity inside the experimental flume is also increasing from 0.8 to 1.6 m/s. The maximum velocity is reached behind the SND in both experimental and numerical flumes. In the in-situ and experimental configurations, the device is porous. A part of the flow goes through the device leading to a smaller velocity increase above the porous device and a smaller energy loss (total pressure drop). The representation of the SND by a bathymetric step thus probably tends to over-estimate the flow acceleration and the associated drag coefficient. In situ, the velocity inside the SND is decreasing which should result in sediment deposit that progressively reduces the porosity. Effectively after one month, the in situ SND can be almost full on sandy deposit [6].

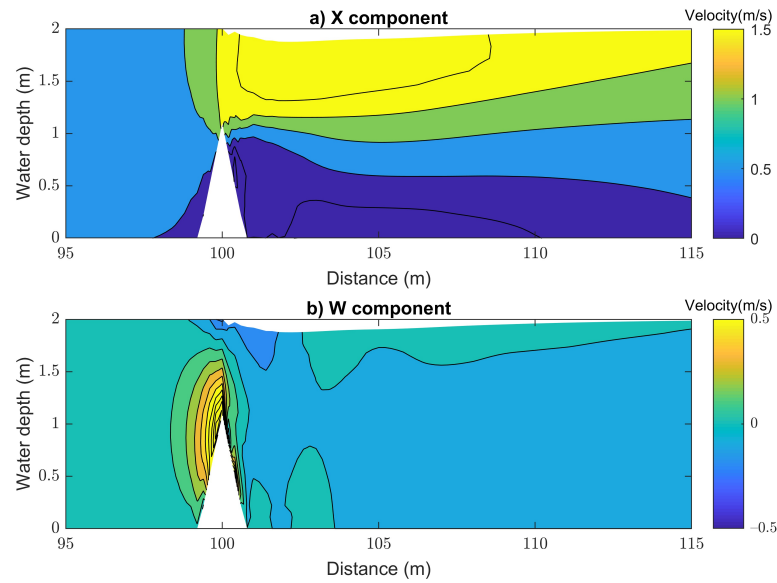


Figure 6. Along (a) and vertical velocities (b) with water depths in numerical experiment induced by the SND.

The evolution of the drag coefficient for the different studied water depths is plotted in Figure 7 in regard of the section ratio before the device and on the device. As the width is constant it corresponds to the ratio of the upstream water depth by the water depth at the step. High water depth leads to less section reduction and less energy losses. It corresponds to high tide configuration. The energy losses increase as power 4 with the water depth ratio. This relationship is conformed with the classical formula of energy losses induced by flow section reduction [30]. From Figure 7, the drag coefficient evolves from 0.3 to 35. The energy losses induced by the device is maximum for low water depth which correspond to the peaks of current during the ebb and the flood and thus when the sediment transport is significant. Figure 7 provides an estimation of the range of values for the drag coefficient requested to build the large scale 2D numerical model.

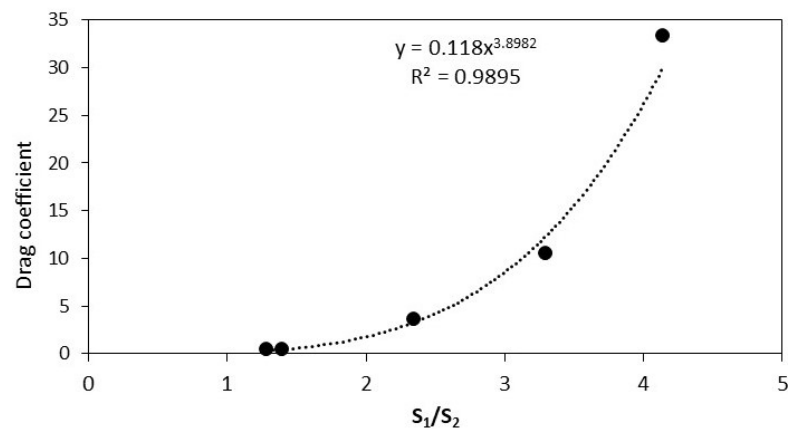


Figure 7. Relationship between drag coefficient and the area ratio from flume numerical, S1 corresponds to the flow area upstream and S2 corresponds to the flow area above the sand nest crest.

4.3. Validation of the 2D Hydrodynamic Model

The performance of the large-scale model has been assessed using data collected in May 2017 (water level and velocity). Figure 8 illustrates the comparison between observed and simulated water levels and velocities for a period of 30 days in May 2017. Model

performance is quantified through root mean square error (RMSE), and predictive skill (SS) introduced by Willmott. [31]. The model score of water level indicates a high value of SS of 0.97 with RMSE of 0.22 m at the Net location. The score of velocity shows a bit overestimate with a value of SS of 0.7 and the RMSE is 0.32 m/s. In general, the model results are able to follow the measurements throughout the neap–spring tidal cycle quite closely. The peak velocity at Net location indicates also a good agreement between observation and simulation.

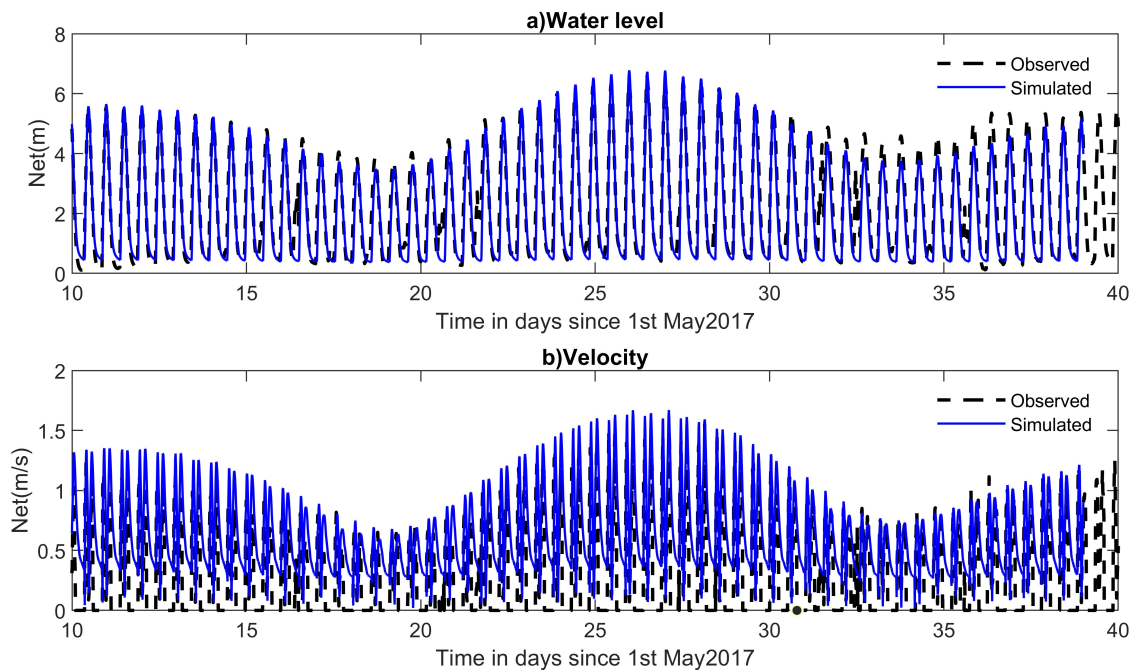


Figure 8. Results of water level (a) and velocity (b) validation at the Net location.

4.4. Influence of the Sand Net on the Residual Current

A 45 days simulation has been performed with or without the SND to evaluate its influences on the bed evolution and associated modifications of the residual currents.

Residual current is estimated over one tidal cycle representing either neap tide or spring tide with and without drag force (Figure 9). Downstream oriented residual currents dominate in both spring (Figure 9a,c) and neap tide (Figure 9b,d) but its magnitude in spring tides is stronger than in neap tides. For the simulation with the drag force, impacts are noticed on the eastern side of the SND in both spring and neap tide. During spring tides (Figure 9c), two branches in the flow pattern are observed creating a zone with low velocity between them (0.05 m/s). However, the velocity is slightly higher at the area of the left side of the SND (0.4 m/s). During neap tides, main branches still maintain around SND but with reduced velocity on the east branch due to influence of the SND.

Residual currents over spring and neap tidal cycle are also extracted at transect T2, cross-section throughout the nets (Figure 10). A large reduction in residual current at the SND is observed both in spring and neap tide. During neap tide, the residual current has been reduced from 0.14 m/s to 0.04 m/s whereas it reduces from 0.25 m/s to 0.07 m/s during the spring tide. Compared to the case without SND, the residual current is divided into two peaks with SND. The residual current increases and reaches the first peak in front of SND (west side, or left side, at distance 100–150 m, Figure 10). Then it decreases due to the SND and forms another peak of velocity on the east side of SND at a distance about 200 m. From Figures 9 and 10, it appears that the core of the SND is creating the region of low velocity behind it.

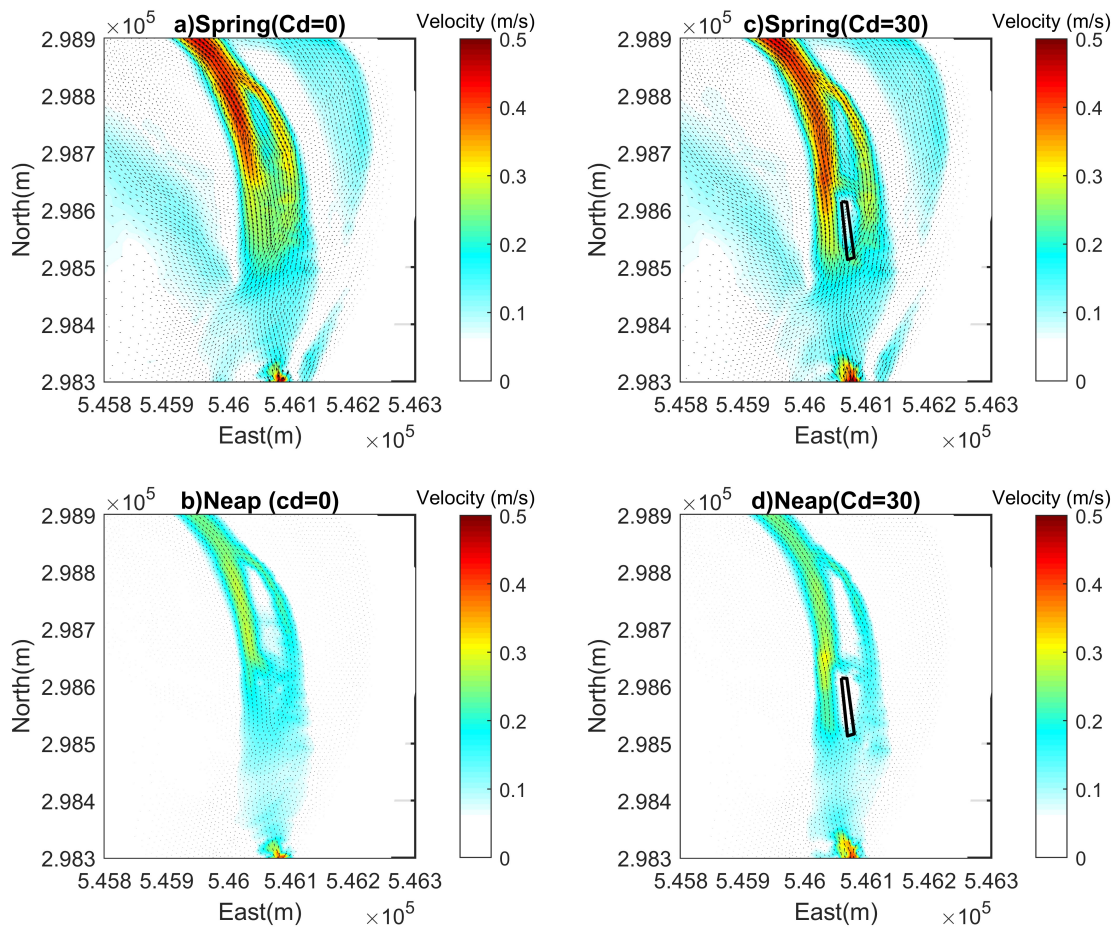


Figure 9. Residual current with and without the SND during spring tide (a,c) and during neap tide (b,d). The back lines depict the location of the SND.

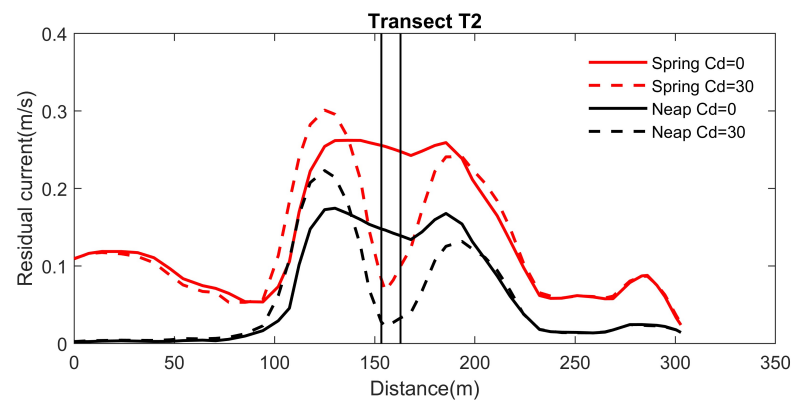


Figure 10. Residual current at cross transect T2 (the SND is located at a distance of 153 m corresponding the reduction zone in velocities indicating by vertical black line).

4.5. Influence of Sand Net Installation on Morphodynamics

Due to the changes in hydrodynamics caused by the SND, morphological development is altered (Figure 11). The effect of SND is stretched out over approximately 400 m along the channel in both directions (upstream and downstream from the net location) with the difference in bed level changes larger than 2 cm.

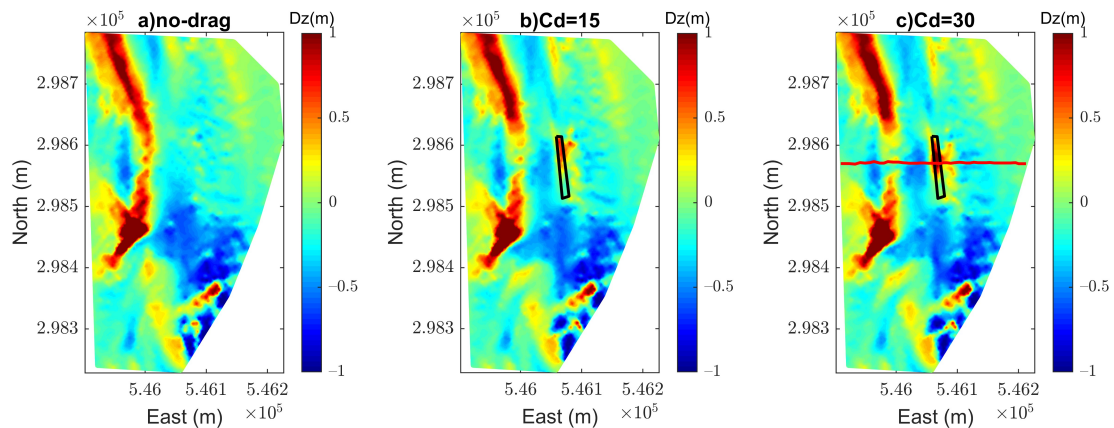


Figure 11. Erosion/sedimentation with different drag coefficients: (a) without drag coefficient $C_d = 0$; (b) with drag coefficient $C_d = 15$; (c) with drag coefficient $C_d = 30$. The black line depicts the location of the SND and the red line indicates location of transect T2. Postive values of D_z indicates sedimentation whereas negative values indicate erosion.

Figure 11 presents the evolution of bathymetry after 45 days simulation considering different drag coefficients (without drag $C_d = 0$; $C_d = 15$, and $C_d = 30$ based on the range of drag coefficient from numerical flume, Section 4.2). The figure illustrates that the SND has contributed to accretion on the right bank of the channel (the area on the right side of the SND) and a deepening of the main channel on the left side of the nets. This erosion/sedimentation pattern displays the same behavior from observed bathymetry (Figure 4a). The model predicts a reduction in velocity and a slight deviation flow around at this location (Figures 9 and 10). This phenomenon leads to a deposition that can be observed behind the sand net and develops further downstream as can be seen in Figure 11b,c. A higher drag force coefficient creates more sedimentation because of more reduction in velocity induced by the SND as shown in Figure 12 (Bed level changes at transect T2). With a drag coefficient of 30, an accretion of approximate 0.8 m is observed behind the SND whereas it reduces to about 0.2 m with a drag of 15 and it shows an erosion of (-0.2 m) in case without drag force (without SND). The deposition behind the SND results from reduction in velocity is observed, this result is quite well comparative with observed bathymetry in Figure 4a. The model confirms that the SND has induced the deposition behind its location and it has an effect on circulation by creating a deflation in current.

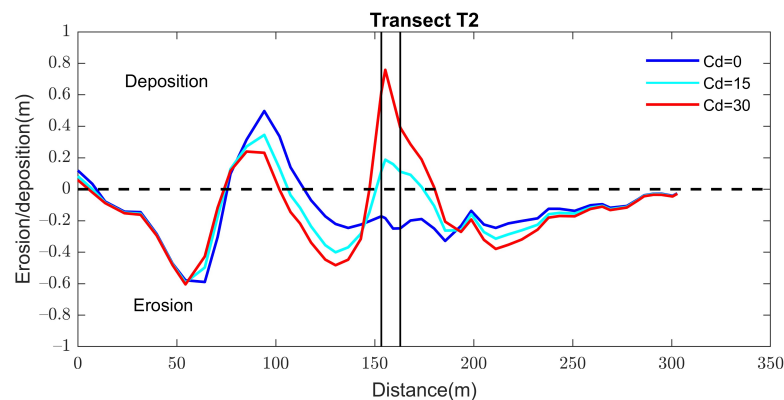


Figure 12. Erosion/sedimentation at the transect T2 with different drag coefficients.

5. Conclusions

A new soft engineering solution, namely the sand net device (SND), has been implemented in the Authie estuary in order to prevent bank erosion by a meandering of a

coastal river. The paper presents the evolution of the morphodynamic over 3 and 6 months after the implementation. In situ monitoring clearly points out sedimentation around the SND and a deepening of the main channel. It has thus successfully maintained the river on its western branch. Numerical modeling allows further analysis and separation of the influence of the SND. From numerical experiments, values of the drag coefficient induced by the SND have been estimated within 0.3 to 30 according to the water depth (high tide corresponds to low drag coefficient). Since the strongest tidal currents have been noticed with low water depth, the strongest energy losses during high transport rate periods. After one and half month, the large-scale model predicts deposition around the SND and modification of the flow circulation.

The large-scale numerical results with SND indicate that, while the nets are able to reduce energy within the study area with a radius effectiveness of around 500 m both directions, upstream and downstream part. The velocity has been reduced and created a deviation in its direction by a circulation around the SND location. The morphological development shows a potential sedimentation around the SND location.

The main patterns are correctly reproduced by the model which could be then used to test different SND configurations. Even if some development could be forecast as 3D modelling and inclusion of waves for longer time scale (year). The way to address the drag force once the SND is full of sand also needs further investigation.

The presence of waves and their subsequent modification has been ignored from this study. The morphological changes are only considered for a short-term period. Consequently, the impact of the nets on long-term morphological development is left for further study.

Author Contributions: Conceptualization, all; methodology, N.H. and A.T.K.D.; software, N.H. and A.T.K.D.; validation, N.H. and A.T.K.D.; formal analysis, N.H. and A.T.K.D.; investigation, N.H.; data treatment, N.H.; writing—original draft preparation, N.H. and A.T.K.D.; writing—review and editing, N.H., A.T.K.D. and P.S.; visualization, A.T.K.D.; supervision, N.H. and P.S.; project administration, N.H. and P.S.; funding acquisition, N.H. and P.S. All authors have read and agreed to the published version of the manuscript.

Funding: This research is part of the ENDURE project funded by Interreg 2 Seas programme 2014–2020 co-funded by the European Regional Development Fund.

Institutional Review Board Statement: Not applicable.

Informed Consent Statement: Not applicable.

Data Availability Statement: The data presented in this study are available on request from the corresponding author. A part of data is not publicly available due to belong to the 3rd party data.

Acknowledgments: The authors gratefully acknowledge the Service d’Hydrographique et d’océanographique de la Marine (SHOM) and the Réseau d’Observations du Littoral Normandie et Haut de France for providing bathymetric and topographic data for this study. The CA2BM is also acknowledged for providing their data and their help to conduct field surveys. This work has been achieved during the Endure (Ensure Dune Resilience) led by Norfolk County Council (<https://www.endure.eu.com/>, accessed on 22 July 2021).

Conflicts of Interest: The authors declare no conflict of interest. Any role of the funders in the design of the study; in the collection, analyses or interpretation of data; in the writing of the manuscript, or in the decision to publish the results.

References

1. Ridderinkhof, W.; Hoekstra, P.; Van der Vegt, M.; De Swart, H.E. Cyclic behavior of sandy shoals on the ebb-tidal deltas of the Wadden Sea. *Cont. Shelf Res.* **2016**, *115*, 14–26. [[CrossRef](#)]
2. Morales, J.A.; Borrego, J.; Jiménez, I.; Monterde, J.; Gil, N. Morphostratigraphy of an ebb-tidal delta system associated with a large spit in the Piedras Estuary mouth (Huelva Coast, Southwestern Spain). *Mar. Geol.* **2001**, *172*, 225–241. [[CrossRef](#)]
3. Monge-Ganuzas, M.; Evans, G.; Cearreta, A. Sand-spit accumulations at the mouths of the eastern Cantabrian estuaries: The example of the Oka estuary (Urdaibai Biosphere Reserve). *Quat. Int.* **2015**, *364*, 206–216. [[CrossRef](#)]

4. Hesp, P.A.; Ruz, M.H.; Hequette, A.; Marin, D.; Da Silva, G.M. Geomorphology and dynamics of a traveling cusped foreland, Authie estuary, France. *Geomorphology* **2016**, *254*, 104–120. [[CrossRef](#)]
5. Bastos, L.; Bio, A.; Pinho, J.L.S.; Granja, H.; da Silva, A.J. Dynamics of the Douro estuary sand spit before and after breakwater construction. *Estuar. Coast. Shelf Sci.* **2012**, *109*, 53–69. [[CrossRef](#)]
6. Sergent, P.; Huybrechts, N.; Smaoui, H. Large Scale Demonstrator of Fishing Nets Against Coastal Erosion of Dunes by Meanders in Authie Estuary (Côte D’Opale—France). In *Estuaries and Coastal Zones in Times of Global Change*; Springer: Singapore, 2020; pp. 573–593.
7. Dobroniak, C. Morphological evolution and management proposals in the Authie Estuary, northern France. In Proceedings of the Dunes Estuaries, Koksijde, Belgium, 19–23 September 2015; Volume 2205, pp. 537–545.
8. Anthony, E.J.; Dobroniak, C. Erosion and recycling of aeolian dunes in a rapidly infilling macrotidal estuary: The Authie, Picardy, northern France. *Geol. Soc. Lond. Spec. Publ.* **2000**, *175*, 109–121. [[CrossRef](#)]
9. Dobroniak, C.; Anthony, E.J. Short-term morphological expression of dune sand recycling on a macrotidal, wave-exposed estuarine shoreline. *J. Coast. Res.* **2002**, *36*, 240–248. [[CrossRef](#)]
10. Cartier, A.; Héquette, A. Variation in longshore sediment transport under low to moderate conditions on barred macrotidal beaches. *J. Coast. Res.* **2011**, *Special Issue 64*, 45–49. Available online: <http://www.jstor.org/stable/26482130> (accessed on 22 July 2021).
11. Marion, C.; Anthony, E.J.; Trentesaux, A. Short-term (≤ 2 yrs) estuarine mudflat and saltmarsh sedimentation: High-resolution data from ultrasonic altimetry, rod surface-elevation table, and filter traps. *Estuar. Coast. Shelf Sci.* **2009**, *83*, 475–484. [[CrossRef](#)]
12. Deloffre, J.; Verney, R.; Lafite, R.; Lesueur, P.; Lesourd, S.; Cundy, A.B. Sedimentation on intertidal mudflats in the lower part of macrotidal estuaries: Sedimentation rhythms and their preservation. *Mar. Geol.* **2007**, *241*, 19–32. [[CrossRef](#)]
13. Michon, D. Dispositif et Système de Protection Contre L’érosion du Littoral. EP 2585640 B1, 6 September 2017.
14. Wang, L.; Shi, Z.H.; Wang, J.; Fang, N.F.; Wu, G.L.; Zhang, H.Y. Rainfall kinetic energy controlling erosion processes and sediment sorting on steep hillslopes: A case study of clay loam soil from the Loess Plateau, China. *J. Hydrol.* **2014**, *512*, 168–176. [[CrossRef](#)]
15. Langendoen, E.J.; Mendoza, A.; Abad, J.D.; Tassi, P.; Wang, D.; Ata, R.; El kadi Abderrezzak, K.; Hervouet, J.M. Improved numerical modeling of morphodynamics of rivers with steep banks. *Adv. Water Resour.* **2016**, *93*, 4–14. [[CrossRef](#)]
16. Huybrechts, N.; Villaret, C.; Lyard, F. Optimized predictive two-dimensional hydrodynamic model of the Gironde estuary in France. *J. Waterw. Port Coast. Ocean. Eng.* **2012**, *138*, 312–322. [[CrossRef](#)]
17. Huybrechts, N.; Villaret, C. Large-scale morphodynamic modelling of the Gironde estuary, France. *Proc. Inst. Civ. Eng. Marit. Eng.* **2013**, *166*, 51–62. [[CrossRef](#)]
18. Santoro, P.; Fossati, M.; Tassi, P.; Huybrechts, N.; Van Bang, D.P.; Piedra-Cueva, J.I. A coupled wave–current–sediment transport model for an estuarine system: Application to the Río de la Plata and Montevideo Bay. *Appl. Math. Model.* **2017**, *52*, 107–130. [[CrossRef](#)]
19. Tassi, P.; Villaret, C.; Huybrechts, N.; Hervouet, J.M.N. Numerical modelling of 2D and 3D suspended sediment transport in turbulent flows. In Proceedings of the Seventh AIRH Symposium River Coastal an Estuarine Morphodynamics, Beijing, China, 6–8 September 2011.
20. Hervouet, J.-M. *Hydrodynamics of Free Surface Flows: Modelling with the Finite Element Method*; John Wiley and Sons Ltd.: West Sussex, UK, 2007, 340p.
21. Egbert, G.D.; Erofeeva, S.Y. Efficient inverse modeling of barotropic ocean tides. *J. Atmos. Ocean. Technol.* **2002**, *19*, 183–204. [[CrossRef](#)]
22. Schureman, P. *Manual of Harmonic Analysis and Prediction of Tides*; US Government Printing Office: Washington, DC, USA, 1958; Volume 4.
23. Audouin, Y.; Benson, T.; Delinares, M.; Fontaine, J.; Glander, B.; Huybrechts, N.; Kopmann, R.; Leroy, A.; Pavan, S.; Pham, C.-T.; et al. Introducing GAIA, the brand new sediment transport module of the TELEMAC-MASCARET system. In Proceedings of the XXVIth TELEMAC-MASCARET User Conference, Toulouse, France, 15–17 October 2019.
24. Van Rijn, L.C. Unified view of sediment transport by currents and waves. II: Suspended transport. *J. Hydraul. Eng.* **2007**, *133*, 668–689. [[CrossRef](#)]
25. Soulsby, R. *Dynamics of Marine Sands*; Thomas Telford: Telford, London, 1997.
26. Villaret, C.; Hervouet, J.M.; Kopmann, R.; Merkel, U.; Davies, A.G. Morphodynamic modeling using the Telemac finite-element system. *Comput. Geosci.* **2013**, *53*, 105–113. [[CrossRef](#)]
27. Brakenhoff, L.; Schrijvershof, R.; Van Der Werf, J.; Grasmeijer, B.; Ruessink, G.; Van Der Vegt, M. From ripples to large-scale sand transport: The effects of bedform-related roughness on hydrodynamics and sediment transport patterns in delft3d. *J. Mar. Sci. Eng.* **2020**, *8*, 892. [[CrossRef](#)]
28. Joly, A.; Pham, C.T.; Andreewsky, M.; Saviot, S.; Fillot, L. Using the DRAGFO subroutine to model Tidal Energy Converters in Telemac-2D. In *Telemac User Club 2015*; Science and Technology Facilities Council: Warrington, UK, 2015.
29. Ross, L.; Sottolichio, A.; Huybrechts, N.; Brunet, P. Tidal turbines in the estuarine environment: From identifying optimal location to environmental impact. *Renew. Energy* **2021**, *169*, 700–713. [[CrossRef](#)]
30. Crane. *Flow of Fluids Through Valves, Fittings, and Pipe*; Technical Paper No. 410 th Printing, 1974; Crane Ltd.: Ongar, UK, 1974.
31. Willmott, C.J. On the validation of models. *Phys. Geogr.* **1981**, *2*, 184–194. [[CrossRef](#)]